THE HURRICANE RAINBAND AND INTENSITY CHANGE EXPERIMENT

Observations and Modeling of Hurricanes Katrina, Ophelia, and Rita

BY ROBERT A. HOUZE JR., SHUYI S. CHEN, WEN-CHAU LEE, ROBERT F. ROGERS, JAMES A. MOORE, GREGORY J. STOSSMEISTER, MICHAEL M. BELL, JASMINE CETRONE, WEI ZHAO, AND S. RITA BRODZIK

Ground-controlled flights, the ELDORA radar, and high-resolution modeling document the historic hurricanes of 2005.

Over the last few decades, the forecasts of tropical cyclone tracks have improved significantly, largely as a result of improvement of large-scale numerical forecast models and satellite observations, whereas relatively little progress has been made in forecasts of hurricane intensity. (Official error trends are documented online at www.nhc.noaa.gov/verification.) Difficulties are that the maximum potential intensity (MPI) of tropical cyclones, estimated from the sea surface temperature and upper-tropospheric temperature and humidity (Emanuel 1988; Evans 1993; DeMaria and Kaplan 1994; Holland 1997), is rarely reached, and the storm intensity frequently undergoes strong fluctuations from one day to the next (e.g., Hurricane Opal 1995; see Lawrence et al. 1998; Krishnamurti et al. 1998; Bosart et al. 2000). Intensity variations during a storm's lifetime are associated with evolution of the storm's internal structure (e.g., Camp and Montgomery 2001) as well as complex interactions with the storm's environment, especially vertical shear (e.g., Elsberry and Jeffries 1996; DeMaria 1996; Frank and Ritchie 1999; Black et al. 2002; Rogers et al. 2003; Chen et al. 2006a), mean flow (e.g., Peng et al. 1999), and low-to-midlevel dry air (e.g., Dunion and Velden 2004). Since the dynamics of the internal structure

AFFILIATIONS: HOUZE, CETRONE, AND BRODZIK—Department of Atmospheric Sciences, University of Washington, Seattle, Washington; CHEN AND ZHAO—Rosenstiel School of Marine and Atmospheric Sciences, University of Miami, Miami, Florida; LEE, MOORE, STOSSMEISTER, AND BELL—Earth Observing Laboratory, National Center for Atmospheric Research, Boulder, Colorado; ROGERS—Hurricane Research Division, Atlantic Oceanographic and Meteorological Laboratory, National Oceanic and Atmospheric Administration, Miami, Florida

CORRESPONDING AUTHOR: Robert A. Houze Jr., Department of Atmospheric Sciences, Box 351640, University of Washington, Seattle, WA 98195-1640
E-mail: houze@atmos.washington.edu

The abstract for this article can be found in this issue, following the table of contents.
DOI:10.1175/BAMS-87-11-1503

In final form 22 June 2006

of the vortex are involved in intensity changes, the physical understanding required for improvements in forecasting tropical cyclone intensity demands detailed observations and high-resolution modeling of the internal structure of the vortex.

The Hurricane Rainband and Intensity Change Experiment (RAINEX) was conceived to address the hurricane internal dynamics via intensive aircraft observations and high-resolution numerical modeling.[1] The premise of RAINEX is that fluctuations in storm intensity derive from the dynamics of and interactions of the eye, eyewalls, and rainbands. The eyewall is a radially outward-sloping circular band of cloud and heavy precipitation surrounding the eye. The rainbands lie radially outside the eyewall and exhibit an inwardly spiraling geometry. RAINEX focused on studying eyewall and rainband structures and behaviors. The principal components of RAINEX were a high-resolution numerical model, Doppler radar measurements from three P3 aircraft, and intensive airborne dropsonde coverage. After years of planning, RAINEX was scheduled in advance for August–September 2005. The aircraft observations were to be staged from Florida in any hurricanes that were within P3 range of Florida. Three storms fell within this time period within range of the RAINEX aircraft: Katrina, Ophelia, and Rita (Fig. 1). Two of these hurricanes, Katrina (Fig. 2) and Rita, were among the most significant, intense, and dangerous storms to occur over the Gulf of Mexico in the history of the United States.[2] Ophelia provided an interesting contrast as a storm that never exceeded category 1, but spent a long time moving up the east coast of the United States. The tracks and intensity of Katrina and Rita resembled the Great Galveston hurricane of 1900 (Larson 1999; Frank 2003). RAINEX was fortunate to obtain excellent data in these historic storms.

SCIENTIFIC BACKGROUND AND OBJECTIVES. Most hurricanes exhibit an eyewall and a set of spiral rainbands (Willoughby et al. 1984; Willoughby 1988). The spiral rainbands exhibit a variety of internal structures, with deep convective cores embedded in stratiform precipitation (e.g., Atlas et al. 1963; Barnes et al. 1983, 1991). Intense hurricanes often exhibit concentric eyewalls, and in these storms intensity changes occur in connection with the eyewall contraction and replacement cycle (Willoughby et al. 1982; Black and Willoughby 1992). A secondary wind maximum sometimes

[1] RAINEX was a collaborative effort of the National Science Foundation, the National Center for Atmospheric Research, the U.S. Naval Research Laboratory, Remote Sensing Solutions, Inc., the National Oceanic and Atmospheric Administration (NOAA)/Atlantic Oceanographic and Meteorological Laboratory Hurricane Research Division, NOAA/Aircraft Operations Center, NOAA/National Environmental Satellite, Data, and Information Service, the University of Washington, and the University of Miami.

[2] Rita and Katrina are currently the fourth and sixth most intense Atlantic hurricanes on record, with minimum observed central pressures of 897 and 902 hPa, respectively.

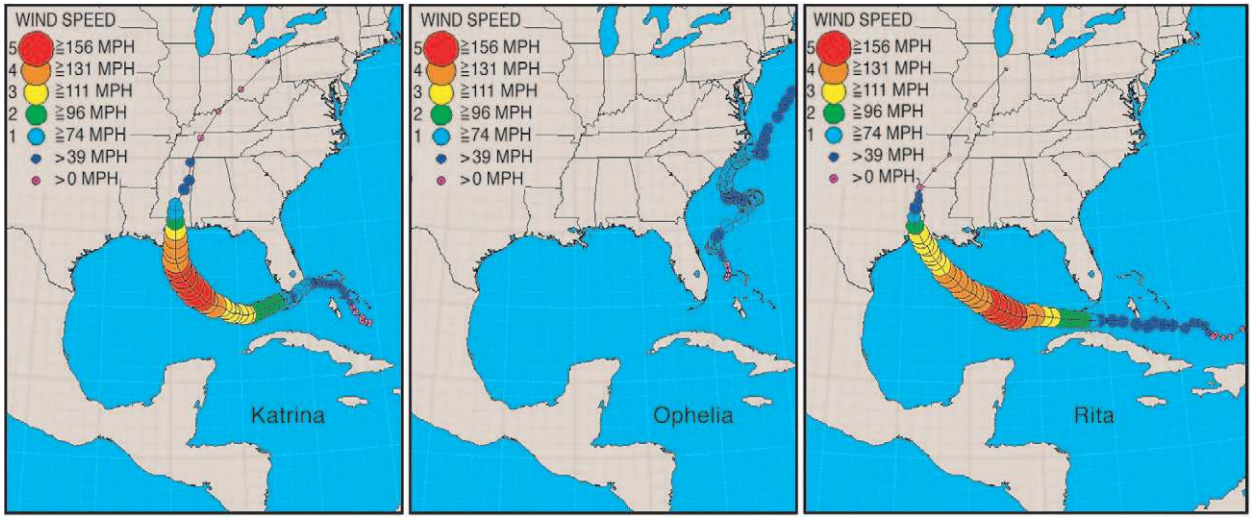

FIG. 1. Hurricane tracks investigated in RAINEX. (Courtesy of R. Sterner and S. Babin of Johns Hopkins University Applied Physics Laboratory.)

occurs within the spiral rainbands (Samsury and Zipser 1995), suggesting that some rainbands are evolving toward an eyewall-like structure. Willoughby et al. (1984) described a frequently observed spiral rainband configuration, based on numerous hurricane flights, which they called the stationary band complex (SBC). It includes an inner eyewall around the center of the storm, one or more principal rainbands, and several secondary rainbands. The principal rainbands are larger than the secondary rainbands and may contain sub-bands. The principal bands often become tangent to the eyewall. At greater distances from the storm center, farther out than the principal bands and secondary bands, outer spiral bands of convection occur. These outer bands are known to be highly convective, and RAINEX aircraft reported some of the roughest flying in the outer convective bands on the outer fringes of the storms.

Fig. 2. Photo taken inside the eye of Hurricane Katrina during the late afternoon (2334 UTC) on 28 Aug 2005 on board the NOAA N43 P-3 aircraft. The aircraft was flying at an altitude of 3500 m. The radially outward slope of the eyewall with increasing height is clearly evident. The darker clouds in the lower part of the image are in the shadow of the eyewall cloud to the west. (Photo by F. Roux.)

The pattern of eyewalls and rainbands in a tropical cyclone is always evolving. Figure 3 is a simplified picture of a typical evolution sequence. However, these patterns are never exactly the same from case to case. In panel (i) of the hypothetical schematic, some disorganized incipient spiral rainbands surround the center of a weak low pressure system. Later, as indicated in panel (ii), some of the rainbands have amalgamated into an eyewall, and a large rainband spirals into and connects with the eyewall. In some intense storms, principal and/or secondary rainbands may evolve into a secondary eyewall, as in panel (iii), which becomes symmetric with an older inner eyewall. The secondary eyewall then becomes the primary recipient of radially inflowing low-level warm, moist air. The inner eyewall collapses as it is cut off from the main low-level inflow (Willoughly et al. 1982; Willoughby 1988), thus accomplishing an "eyewall replacement," as shown in panel (iv). During this stage, the cyclone intensity decreases rapidly. The radius of the new eyewall then contracts,

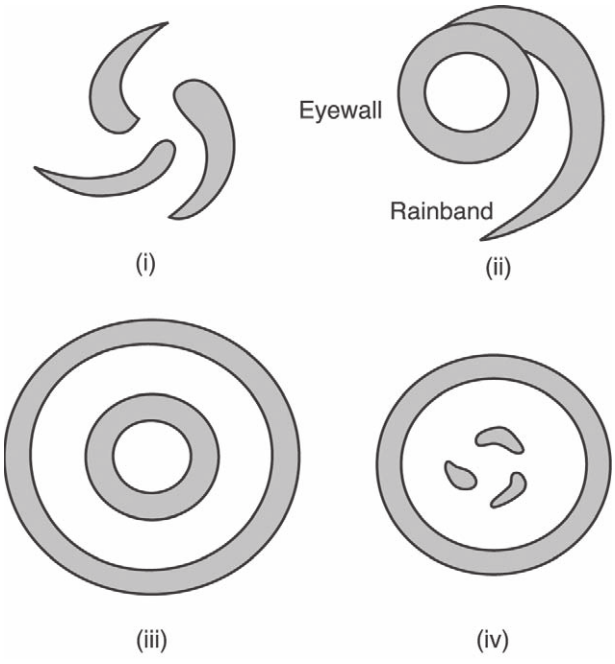

Fig. 3. Simplified schematic of four stages of rainbands and eyewall in a tropical cyclone. The gray areas indicate precipitation, as would be seen on a radar. Rainbands have spiral geometry; eyewalls exhibit circular geometry.

and the cyclone reintensifies. RAINEX was designed to examine how intensity changes of the hurricane appear to be related to the variations of eyewall/rainband structure, including the evolution of spiral bands into eyewalls and interactions of eyewalls and rainbands.

The hurricane inner-core region has been investigated extensively in previous observational studies. Aircraft observations have documented the eyewall region, including concentric eyewall cases (Willoughby et al. 1982; Jorgensen 1984a,b; Jorgensen et al. 1985; Marks and Houze 1984, 1987; Willoughby 1990; Marks et al. 1992; Houze et al. 1992; Gamache et al. 1993; Black and Willoughby 1992; Reasor et al. 2000). Observational studies have also explored rainbands (Barnes et al. 1983; Barnes and Stossmeister 1986; Powell 1990a,b; Samsury and Zipser 1995). Samsury and Zipser (1995) found that about 30% of outer rainbands contained a secondary horizontal wind maximum (SHWM), similar to the eyewall. This result suggests that spiral rainbands might evolve into eyewall-like structures. These past studies have drawn some limited conclusions regarding the interactions of the outer rainbands with the inner-core dynamics. For example, Barnes et al. (1983) and Powell (1990a,b) found that the rainband downdrafts can sometimes lower the low-level θ_e of air approaching the eyewall. These past observational studies, however, have not exhaustively explored how the hurricane outer rainbands interact with the storm's inner core, resulting in storm intensity changes.

Theoretical and modeling studies are useful tools for understanding the physical nature of the rainbands and their interaction with one another and the vortex core (eyewall) region. Idealized modeling studies have attempted to explain the existence of the spiral rainbands. Kurihara (1976) and Willoughby (1978) proposed that internal gravity–inertia waves are responsible for the outward-propagating spiral rainbands. More recently, Guinn and Schubert (1993), using an *f*-plane shallow-water model, conducted a series of numerical experiments and concluded that the hurricane rainbands can be explained by the potential vorticity (PV) redistribution or PV wave-breaking and vortex-merging processes. Montgomery and Kallenbach (1997) developed a theoretical framework for 2D phase and group velocities for vortex Rossby waves and described the outward propagation of rainbands as vortex Rossby waves. Chen and Yau (2001) used a nonhydrostatic, full physics mesoscale model to confirm that the rainbands simulated in the model have the characteristics of vortex Rossby waves. Chen et al. (2003) further confirmed the characteristics of vortex Rossby waves by using empirical normal-mode techniques.

Theoretical and modeling studies have further identified a number of mechanisms that may be responsible for structure and intensity changes in the inner core of a symmetric tropical cyclone. Extending a theory of Eliassen (1951) for simple balanced vortices to tropical cyclones, Shapiro and Willoughby (1982) showed how eyewall heating leads to low-level wind intensification, warming in the eye, and lower surface pressures.

Asymmetric forcing has also been studied as a possibly important intensification mechanism, whereby asymmetries in the wind field cause inward fluxes of angular momentum as they are sheared by the symmetric flow (Pfeffer 1958; Carr and Williams 1989). As storms intensify, asymmetries in the form of vortex Rossby waves can lead to polygonal eyewalls (Muramatsu 1986), mesovortices (Marks and Houze 1984; Black and Marks 1991), and even a complete breakdown and rearrangement of the inner-core structure (Schubert et al. 1999; Nolan and Montgomery 2002). Such an evolution has been observed directly (Kossin and Eastin 2001).

Secondary eyewall formation and associated eyewall replacement are an especially important dynamical process related to storm intensity change. While secondary wind maxima are another potential source of dynamic instability, Kossin et al. (2000) showed that a prescribed outer ring of maximum wind could be stabilized by the strong radial shear of the azimuthal wind associated with the inner-core vortex. Mechanisms for the formation of secondary wind maxima and concentric eyewalls remain a focus of research. As will be described in the section titled "Observations and modeling of Hurricane Rita (2005)" the RAINEX flights in Hurricane Rita documented an eyewall replacement and concentric eyewalls.

A useful concept in understanding symmetric and asymmetric tropical cyclone dynamics is the conservation of PV under balanced or "quasibalanced" vortex conditions (Shapiro and Montgomery 1993). It is a premise of RAINEX that observations indicating the detailed pattern of PV, and its production via diabatic heating, are critical to understanding how inner-core asymmetries, spiral bands, and secondary eyewalls may or may not cause changes in intensity and structure. Montgomery and Enagonio (1998) suggested that finite-amplitude PV anomalies induced by deep convective cluster episodes would lead to vortex intensification. May and Holland (1999) estimated

PV production in stratiform regions of rainbands and suggested that PV anomalies formed in this way could contribute to intensification as they spiral into the vortex inner core. The shearing deformation can stretch the vorticity into filaments that spiral toward the center of the tropical cyclone (e.g., Holland and Dietachmayer 1993). Wang (2002) found that inward-intruding outer rainbands interact with the eyewall circulation and may occasionally weaken the storm intensity. Nolan and Grasso (2003) simulated the hydrostatic and gradient wind adjustment process in which heating anomalies generate balanced PV anomalies and found that the PV structures caused by asymmetric heating were associated with intensification.

These studies suggest that direct measurements of finescale wind, temperature, and vorticity fields will be critical to resolving the role of eyewalls and rainbands in determining cyclone intensity changes. RAINEX was designed to test this hypothesis by using a high-resolution numerical model in conjunction with carefully targeted multiaircraft dual-Doppler radar measurements and intensive dropsondes *both* near the eyewall *and* in the outer rainband regions of tropical cyclones. These measurements will allow us to determine the small-scale pattern of vorticity associated with the internal structures of eyewalls and rainbands. The observed patterns will be related to the evolving distribution of vorticity and PV in high-resolution model simulations, which will indicate how the eyewalls, rainbands, and their interactions contribute to variations in tropical cyclone intensity.

RAINEX AIRCRAFT AND MODEL FACILITIES. RAINEX employed three P3 aircraft, equipped with Doppler radar and dropsonde capability (Fig. 4). All three aircraft were based at MacDill Air Force Base in Tampa, Florida, at the headquarters of the NOAA/Aircraft Operations Center (AOC). Flights were controlled from the RAINEX Operations Center (ROC) at the Rosenstiel School of Marine and Atmospheric Science (RSMAS) of the University of Miami (UM). Two of the aircraft participating in RAINEX aircraft were the NOAA P3 aircraft, referred to as N42 and N43. The third P3 aircraft in RAINEX was the U.S. Naval Research Laboratory (NRL) P3. The dual-Doppler radar system at the NRL P3 was the National Center for Atmospheric Research (NCAR) dual-beam Electra Doppler Radar (ELDORA; Hildebrand et al. 1996; Wakimoto et al. 1996), which is noted for its fine horizontal sampling resolution of about 0.4 km. In RAINEX, N43 was equipped with the original NOAA single-parabolic antenna, which accomplished dual-Doppler observation by alternately scanning the antenna fore and aft, while N42 carried two French-built flat-plate antennas that scanned at a fixed 20° fore and aft of the plane perpendicular to the fuselage, and accomplished dual-Doppler observations by switching transmission between antennas during successive scans (Frush et al. 1986; Hildebrand 1989; Jorgensen and Smull 1993; Jorgensen et al. 1996). The along-track sampling resolution is about 1.5 km with the NOAA P3 radars. These along-track sampling rates lead to horizontal resolvable wavelengths of 2 and 8 km for the dual-Doppler analyses with the ELDORA and NOAA P3 aircraft, respectively. RAINEX was the first time that the higher-resolution ELDORA radar has been used in tropical cyclones. All three aircraft were supplied with enough dropsondes to obtain soundings at intervals of 5–10 min when the radars were observing rainbands and eyewalls. NRL, NOAA, and NCAR engineering support staff for the aircraft and instruments was located primarily at MacDill but also in Miami, Florida, and Boulder, Colorado.

The aircraft measurements were supported by real-time high-resolution numerical model forecasts of each hurricane. These forecasts were performed with the UM high-resolution, vortex-following coupled ocean–atmosphere version of the nonhydrostatic fifth-generation Pennsylvania State University (PSU)–NCAR Mesoscale Model (MM5) coupled with a wave model and an ocean model. A mini-ensemble

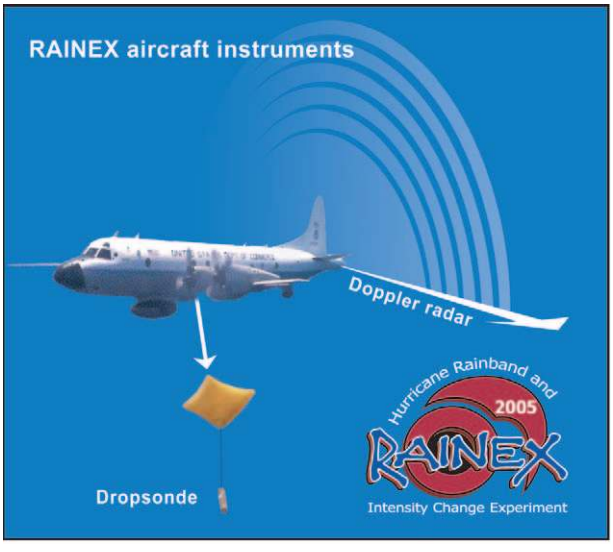

FIG. 4. The primary instruments of RAINEX were dropsondes and Doppler radar measurements obtained on flights of the NOAA and NRL P3 aircraft.

of the MM5 5-day forecasts was made daily using large-scale model forecasts from four different operational centers as initial and lateral boundary conditions. The NCEP Global Forecast System (GFS), the Naval Operational Global Atmospheric Prediction System (NOGAPS), the Canadian Meteorological Centre (CMC), and the Geophysical Fluid Dynamics Laboratory (GFDL) large-scale models were included. In addition, experimental forecasts with the NCAR Weather Research Forecast (WRF) model were conducted at RSMAS/UM and NCAR. MM5 forecasts were made when there was an active tropical storm with the vortex-following nested grids at 15-, 5-, and 1.67-km resolution. The model forecast output was used daily in flight planning for RAINEX. In postanalysis, high-resolution model simulations of the hurricanes observed during RAINEX will be conducted using the fully coupled atmosphere wave–ocean model developed at RSMAS/UM (Chen et al. 2006b, manuscript submitted to *Bull. Amer. Meteor. Soc.*). The aircraft data will be compared to the model output to determine the accuracy of the model real-time forecasts and simulations. The model will thus extend the diagnosis beyond what would be possible from the data alone.

GROUND–AIR DATA FLOW, PROJECT COMMUNICATIONS, AND AIRCRAFT COORDINATION. RAINEX took a novel approach to obtaining a dataset relevant to tropical cyclone intensification. The basic idea was to target the airborne radar and dropsondes in key parts of the tropical cyclone under the guidance of real-time high-resolution model forecasts and by coordination of the flights by ground coordinators connected via satellite communications to the three RAINEX P3 aircraft. An ROC was set up at RSMAS in Miami. The RAINEX Principal Investigators (PIs), forecasters, aircraft operators, and facility engineering staff held a scheduled daily conference call, which originated from the ROC and involved project personnel in Miami, Tampa, Boulder, and other locations. A conference call addressed the forecast for the next 24–36 hours, availability of facilities, and possibilities for flight operations for the next day. At the end of the call, the PIs decided whether the next day would be a possible flight day. On the day of a flight, a preflight conference call of the same parties examined the current state of the target storm and the high-resolution MM5 forecast was evaluated to determine the probable evolution of the internal structure of the storm during the flight. Based on this information, the PIs developed the basic flight plan of the day, or canceled flights for the day. Once in the air, all the participating aircraft were in contact with the ROC via Internet chat (Fig. 5) using air-to-ground satellite links. Also joining the chat were facility engineering support staff in Tampa, Boulder, and Miami. The Internet chat connection allowed the ROC to guide the simultaneous coordination of all the aircraft. In addition to the chat exchange, radar data being obtained by N42 and N43 with their horizontally scanning lower-fuselage radars were transmitted by satellite link to the ROC. The position of the aircraft was also transmitted to the ROC, where a continually updated com-

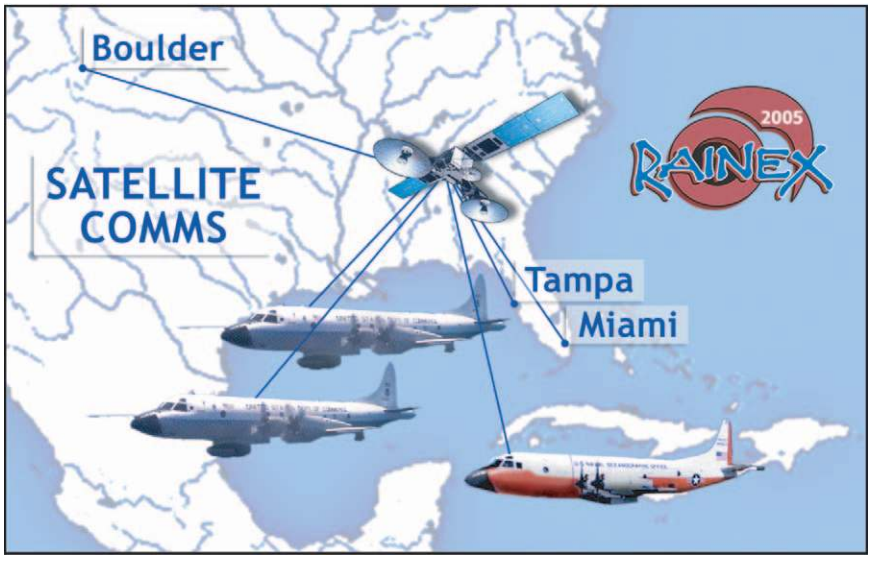

FIG. 5. Satellite communications were crucial to RAINEX. Radar and flight track data from the aircraft were communicated via the satellite links to the RAINEX Operations Center in Miami where they were combined into a real-time composite radar–satellite flight track map. The PIs at the ROC in Miami in turn used the real-time composite map to guide and coordinate the aircraft flights by communicating with the airborne mission scientists over the satellite communication links via Internet chat. NOAA, NCAR, and NRL flight support staff in Tampa and Boulder used the satellite-based Internet chat to troubleshoot and maintain instruments and communications equipment on board the aircraft.

posite map of satellite, airborne radar data from N42 and N43, coastal Weather Surveillance Radar-1988 Doppler (WSR-88D) data (when flights were close to the U.S. coast), and flight tracks of all three aircraft was constructed. The engineering support allowing this data transfer to occur between the ROC and the aircraft was a collaborative effort of the NOAA/National Environmental Satellite, Data, and Information Service (NESDIS), NCAR, and Remote Sensing Solutions, Inc. The platform for the construction of the continually updated composite mission map was the NCAR Zebra visualization and analysis software (Corbet et al. 1994). The composite map was based on the radar data transmitted from the aircraft to the ROC every 5 min. In the composite map, the radar echo in one part of the storm was remembered and included even after the aircraft proceeded to a different part of the storm. Thus, as the aircraft flew to different parts of the storm, the composite map painted the radar echo pattern over most of the storm. This map was continually updated and displayed for the RAINEX PIs in the ROC and provided an excellent overall picture of the distribution of eyewalls and rainbands. This view was much more complete than the radar view available on any individual aircraft, and the PIs in the ROC were therefore able to optimize the flight tracks of all the aircraft. Since the NRL P3 does not have a horizontally scanning radar, a portion of the composite map centered on the NRL P-3 was transmitted to that aircraft at intervals of ~10 min to aid the onboard flight crew and scientists. Figure 6 is an example of a map created at the ROC and transmitted to the NRL P3 in real time.

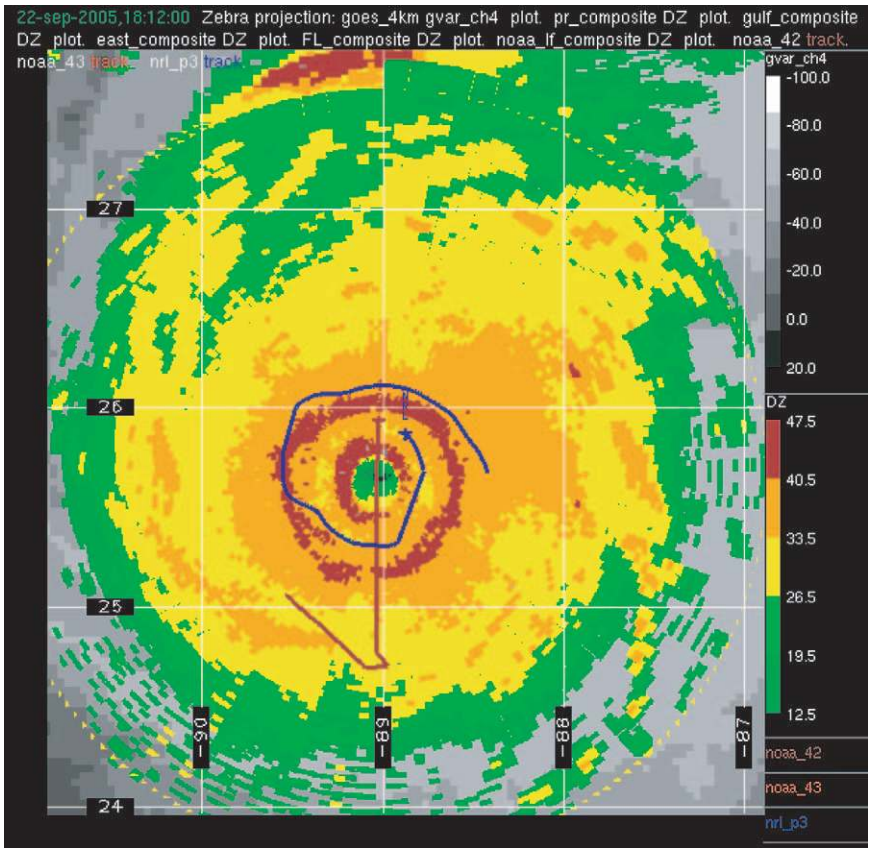

Fig. 6. Example of the real-time radar–satellite flight track overlay transmitted from the ROC to the NRL aircraft in RAINEX. This example is from Hurricane Rita, when the NRL aircraft (blue) and N42 aircraft (rust) were flying near the eye of the storm, when a secondary eyewall was present. Color shading is radar data. Gray shades are satellite.

TARGETING THE EYEWALLS AND RAINBANDS. A basic premise of RAINEX was that tropical cyclone intensity changes are associated at least in part with the interactions of the mesoscale circulations of eyewalls and rainbands. Therefore, the RAINEX flight program aimed to obtain mesoscale air motions and thermodynamics via dual-Doppler radar and intensive dropsonde data within and in the immediate vicinity of the most prominent rainbands and eyewalls that presented themselves on the lower-fuselage radars of N42 and N43. Figure 7 illustrates the basic RAINEX flight strategy by superimposing basic flight track models on the idealized eyewall/rainband pattern of Willoughby (1988).

Plan A in Fig. 7 was the default pattern that RAINEX attempted to employ. In this module, two aircraft would fly coordinated tracks on either side of a rainband, to provide "quad-Doppler" coverage, which oversamples the wind components in the rainband to give the most reliable wind pattern (Jorgensen et al. 1996) and expands horizontal coverage of the rainband beyond the effective range of a single airborne radar. The other aircraft would provide information on the eyewall and eye via a

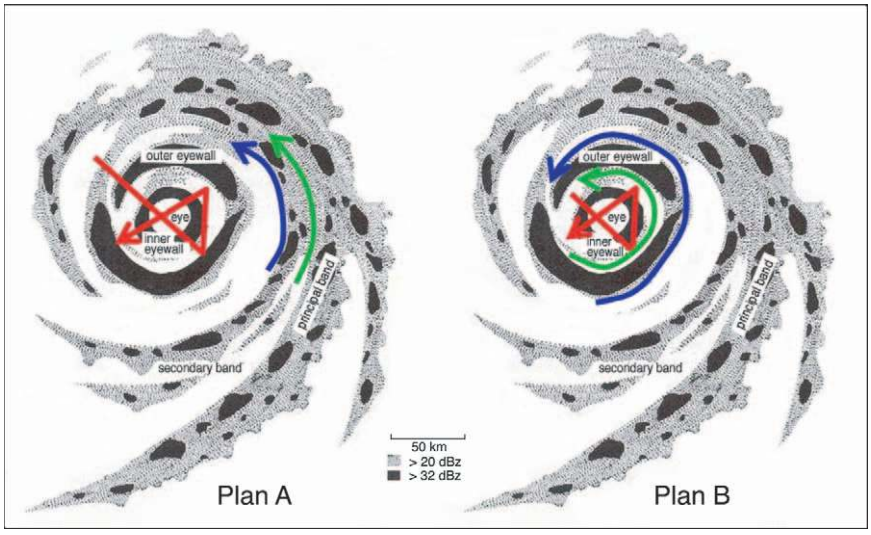

Fig. 7. Idealized flight track plans for the P3 aircraft in RAINEX. The idealized tracks are overlaid on the schematic hurricane radar echo pattern of Willoughby (1988). Colors indicate different aircraft.

"figure four" pattern. A major goal of RAINEX was the joint, near-simultaneous dual-Doppler coverage of both the rainband and eyewall.

Plan B in Fig. 7 was for use in the event that the aircraft would arrive during an eyewall replacement characterized by both an inner and outer eyewall. In that case the rainband aircraft would be moved inward to document the secondary (outer) eyewall via circumnavigation legs on the inside and outside edges of the outer eyewall. As it happened, the aircraft arrived in Hurricane Rita on 22 September 2005 just as concentric eyewalls were forming, and plan B was implemented (e.g., Fig. 6).

Although the patterns in Fig. 7 are idealizations, they served as a conceptual model to guide the direction of aircraft flights in the real storms observed in RAINEX. Each storm had a unique distribution of eyewall and rainband radar echoes. The PIs took into account the actual radar echo pattern seen in the composite map in the ROC as they directed the aircraft into flight patterns as similar to those in Fig. 7 as was possible. In practice, this guidance from the ROC was accomplished over Internet chat as a collaboration between the PIs in the ROC and the airborne mission scientists on board each aircraft. The experience of the airborne mission scientists (especially R. Rogers and M. Black of HRD, B. Smull of the University of Washington, W.-C. Lee of NCAR, D. Jorgensen of the NOAA/National Severe Storms Laboratory, and P. Chang of NESDIS) was critical in coordinating these patterns in communication with the ROC. The real-time high-resolution MM5 forecasts at RSMAS helped the PIs anticipate changes in the eyewall and rainband patterns as the flight progressed and thus helped determine the optimal track guidance to the aircraft from the ROC. This approach to guiding and positioning the aircraft by applying as strictly as possible the idealized flight track plans in Fig. 7 to the actual mesoscale rainband and eyewall structures led to a consistent dataset for the whole field program.

The flight legs in Fig. 7 position the aircraft for optimal multiple-Doppler radar coverage of the eyewalls and rainbands. In addition, dropsondes were launched every 5–10 min (or roughly 30–65 km) along these legs. The dropsondes provided key thermodynamic information and documented the flow on the perimeters of rainbands and eyewalls. In addition, dropsondes documented the thermodynamic structure in the eye and in the "moat" region between inner and outer eyewalls.

SUMMARY OF THE DATASET OBTAINED IN RAINEX. From its inception, RAINEX has been dedicated to a comprehensive data management strategy that makes readily available the entire research dataset as well as operational data products used to guide the project in the field. A central access point for the entire record and archive of data collected in RAINEX is online at www.eol.ucar.edu/projects/rainex. In this seciton we briefly summarize the highlights of this record. Table 1 lists each day for which data were archived for Katrina, Ophelia, and Rita and the strength of the storms during each flight operation, the participating aircraft, and the general location of the research flights when they occurred. A more comprehensive set of reports and imagery of all aspects of the RAINEX operations and dataset is available online as the RAINEX Field Catalog at http://catalog.eol.ucar.edu/rainex. The Field Catalog, maintained by the NCAR Earth Observing Laboratory (EOL) includes daily operations reports, facility status summaries, as well as a complete inventory of and access to the diverse set of products used by the project to plan and conduct operations. The permanent and continually updated RAINEX Data Archive,

also maintained by EOL, is located online at http://data.eol.ucar.edu/master_list/?project=RAINEX. Investigators interested in the RAINEX dataset may access and order data via this site. The home page of the Web site displays a table showing all the RAINEX-related data and products available from aircraft, radar, upper-air, model, and surface network arrays. This table further indicates procedures for ordering data, includes the latest posting dates of data and products, and provides links to supporting dataset documentation.

An important part of the RAINEX legacy are the science reports that were prepared by members of the science team in the field and further updated in subsequent months. These reports are located online at http://catalog.eol.ucar.edu/rainex/missions.html. They provide a key first glance at the impressions of the missions from a scientific and operations perspective and give a glimpse of the impressive high-resolution dataset collected inside the storms. They also include preliminary model results from specialized mesoscale models being used to simulate storm structure and forecast its evolution.

The NRL, N42, and N43 aircraft flew more than 200 aircraft research flight hours in the storms listed in Table 1. Remarkably, dual-Doppler radar data were collected nearly flawlessly by all three of these aircraft during all of these hours. The result is an enormous and very high quality dual-Doppler radar dataset. These flights were carried out as a merged collaborative effort of the NOAA/Atlantic Oceanographic and Meteorological Laboratory/Hurricane Research Division (HRD), AOC, NESDIS, NCAR, the Naval Research Laboratory, Remote Sensing Solutions, Inc., the University of Washington, and the University of Miami.

RAINEX collected a voluminous set of hurricane upper-air soundings. Dropsondes released from the P3 aircraft were targeted for optimal coordination with the dual-Doppler radar data in rainbands and eyewalls, with ground-based guidance from the ROC. This unprecedented focused set of dropsondes internal to tropical cyclones is a major contribution of RAINEX. The three RAINEX turboprop aircraft and NOAA G-IV released approximately 600 dropsondes in the three investigated storms. These dropsondes were targeted to optimize coordination with the dual-Doppler radar data, as described above. This count of 600 dropsondes does not include those dropsondes released by the U.S. Air Force (USAF) Weather Reconnaissance Wing flights. In addition, the RAINEX dataset will contain all U.S. National Weather Service rawinsondes taken on the U.S. mainland and Caribbean islands as well as soundings from other Caribbean nations, Mexico, and Senegal. The operational rawinsondes will add another 250 rawinsondes to the RAINEX dataset. Raw, processed, and standard skew-*T* plots from all these platforms and sites will be included in the Field Catalog and RAINEX Data Archive at EOL.

Table 1. Summary of RAINEX cases. Hurricane intensity values account for values when the aircraft were in the vicinity. Science reports and additional data are available from the RAINEX data archive at NCAR/EOL. Intensity categories for hurricanes are listed according to the Saffir–Simpson scale. T.D. indicates a tropical depression; T.S. indicates a tropical storm; Cat indicates category.

Storm name	Intensity	Date	Aircraft facilities	Location
Katrina	T.S./Cat 1	25 Aug	NRL, N43	Atlantic Ocean, offshore of Miami, FL
Katrina	Cat 1	26 Aug		Southwestern Florida
Katrina	Cat 2/3	27 Aug	NRL, N43	Eastern Gulf of Mexico
Katrina	Cat 5	28 Aug	NRL, N43	Central Gulf of Mexico
Katrina	Cat 4/5	29 Aug	N43	Landfall, Louisiana, Alabama, and Mississippi
Ophelia	T.D./T.S.	6 Sep	NRL, N42	Western Bahamas
Ophelia	Cat 1	9 Sep	NRL, N43	Atlantic Ocean, east of Jacksonville, FL
Ophelia	T.S./cat 1	11 Sep	NRL, N42, N43	Atlantic Ocean, east of Charleston, SC
Rita	T.S.	19 Sep	NRL, N43	Southern Bahamas, Cuba
Rita	Cat 1	20 Sep	N43	South Florida, Cuba, Florida Keys
Rita	Cat 4/5	21 Sep	NRL, N43	South-central Gulf of Mexico
Rita	Cat 4	22 Sep	NRL, N42, N43	Central Gulf of Mexico
Rita	Cat 3/4	23 Sep	NRL, N42, N43	Northern Gulf of Mexico, south of New Orleans, LA

A set of selected real-time MM5 and WRF forecasts, along with some global model forecasts, during RAINEX are available online at http://catalog.eol.ucar.edu/cgi-bin/rainex/model/index. A link to this site is on the home page of the Field Catalog. The mini-ensemble MM5 forecasts using four different large-scale model forecast fields as initial and lateral boundary conditions can also be found online at http://orca.rsmas.miami.edu/rainex.

The RAINEX dataset includes a variety of satellite data downloaded during the time period of the project. The images and data are focused on the Atlantic, Gulf of Mexico, and the Caribbean area, and special high-resolution movable data windows were employed during each investigated cyclone. One of the satellite datasets specifically downloaded and archived was the three-dimensional, high-resolution Tropical Rainfall Measuring Mission (TRMM) satellite during its overpasses of the cyclones investigated in RAINEX. An example of the TRMM data can be seen in the discussion of Hurricane Rita in the next section.

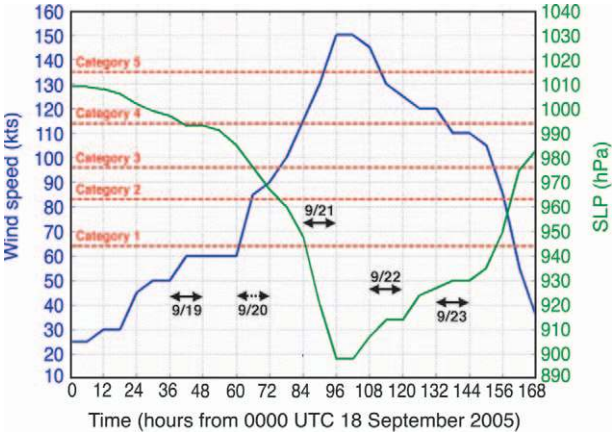

Fig. 8. Observed minimum sea level pressure (green) and maximum surface wind speed (blue) in Hurricane Rita from 0000 UTC 18 Sep to 0000 UTC 25 Sep 2005 (data from the National Hurricane Center). The arrows indicate the four time periods of the RAINEX missions on 19, 21, 22, and 23 Sep, and one non-RAINEX mission on 20 Sep.

OBSERVATIONS AND MODELING OF HURRICANE RITA (2005). Hurricane Rita (2005) showcases the RAINEX dataset. Figure 8 shows the timeline of the five aircraft missions in Rita: during her tropical storm phase (19 and 20 September), while rapidly intensifying from category 4 to 5 (21 September), while rapidly weakening from category 5 to 4 (22 September), and just prior to landfall as a category 3 hurricane (23 September). On 20 September, the real-time high-resolution MM5 5-day forecast indicated the development of a major hurricane with concentric eyewalls and eyewall replacement in the Gulf of Mexico before landfall. Targeted multi-aircraft missions were planned accordingly for the next few days.

During the rapidly intensifying phase on 21 September, plan A flights (recall the section titled "Targeting the eyewalls and rainbands") documented the structure of the eyewall and rainbands. Figure 9 illustrates the close coordination

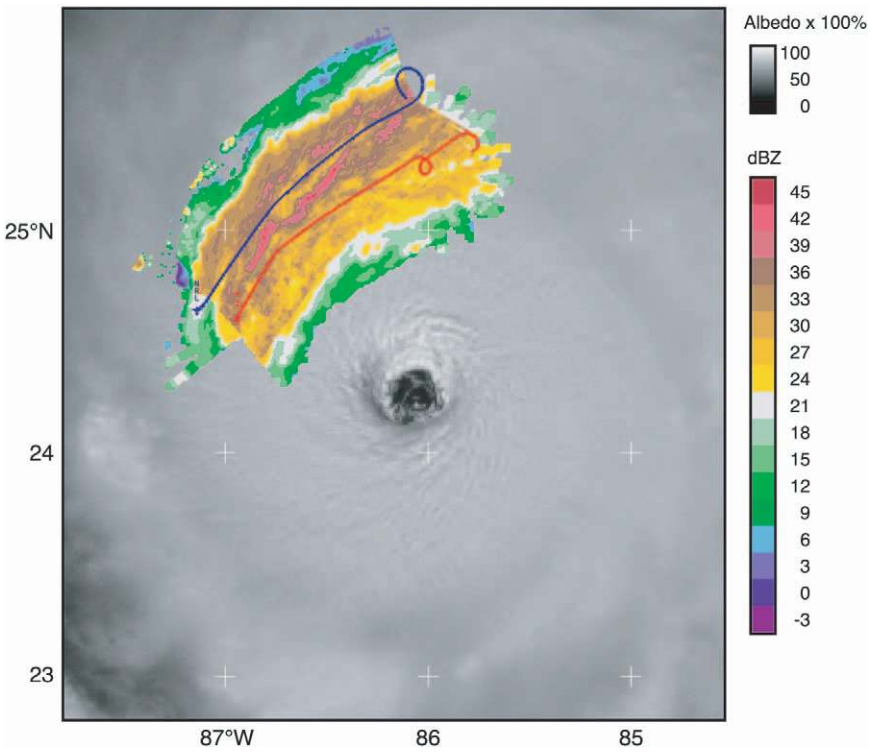

Fig. 9. ELDORA and N43 radar reflectivity composites obtained between 1739 and 1756 UTC 21 Sep 2005 superimposed on visible satellite data for Hurricane Rita. Flight tracks of N43 (red) and NRL (blue) ending at the aircraft icons are superimposed.

achieved with two aircraft performing a synchronized quad-Doppler pattern to observe a rainband in the northwest quadrant of the storm. The radar data in this figure show the detailed internal structure of the rainband, as seen by the ELDORA radar on the NRL P3 aircraft. The small-scale reflectivity maxima seen in the ELDORA data were narrow, elongated cores at an oblique angle to the larger rainband.

Figure 10 shows a simultaneous sampling of the principal rainband in the northeast quadrant of the cyclone by the NRL P3 and ELDORA, and a probing of the eyewall and eye by N43. Figure 11 shows a cross section of the radar reflectivity data collected at this time. The eyewall echoes were deep tilting outward. The melting signature in the rainband echo shows the increase of the 0°C height toward the warm center of the cyclone. Figure 12a shows raw dropsonde data obtained in the eye. It indicates a strong subsidence inversion and weak winds. Figure 12b shows a nearly saturated and moist-adiabatic sounding obtained during a penetration of the eyewall. The warm center of the storm, stable eye, and outward-tilting and moist-adiabatic eyewall are all consistent with the structure of a healthy symmetric hurricane (Emanuel 1986; Houze 1993, chapter 10).

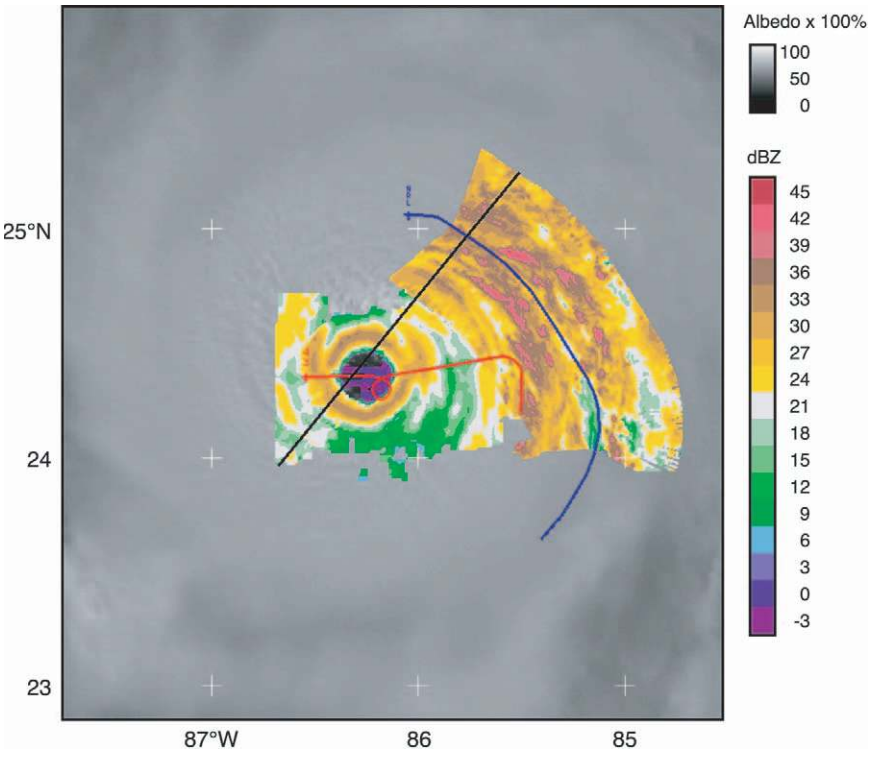

Fig. 10. ELDORA and N43 radar reflectivity composites obtained between 1915 and 1925 UTC 21 Sep 2005 superimposed on visible satellite data for Hurricane Rita. Flight tracks of N43 (red) and NRL (blue) ending at the aircraft icons are superimposed. Black line indicates location of cross section in Fig. 11.

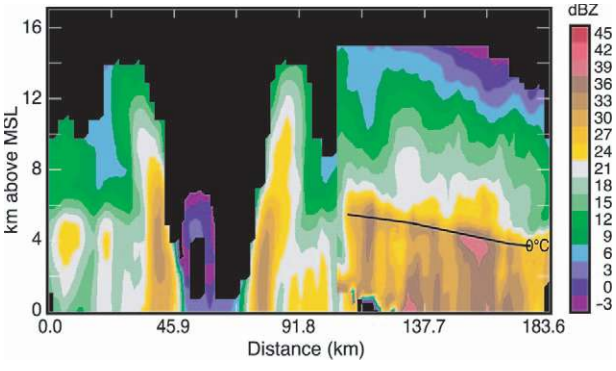

Fig. 11. ELDORA and N43 interpolated radar reflectivity cross section along the straight black line in Fig. 10.

Shortly after the flights on 21 September, Rita reached category 5 intensity with a minimum observed sea level pressure of 897 hPa (Fig. 8). Overnight and into the next day, Rita weakened in connection with an eyewall replacement process. The UM high-resolution model captured the formation of the concentric eyewalls and the eyewall replacement, except the timing was about 6–8 hours earlier than the observations. Figure 13 shows a time–radius diagram of the azimuthally averaged rain rate and wind at about the 3-km level from the 5-day UM high-resolution model forecast initialized at 0000 UTC 20 September and using the NOGAPS forecast field as the lateral boundary conditions. This plot summarizes the evolution of the primary eye and eyewall, formation of the secondary eyewall, and the eyewall replacement. The primary eye and eyewall contracted as Rita intensified on 21 September. The development of the outer rainbands into a secondary eyewall was evident as early as 1800 UTC 21 September (Fig. 13a). The associated secondary wind maximum became obvious a few hours later (Fig. 13b). Subsequently the outer rainband strengthened and became a clear second-

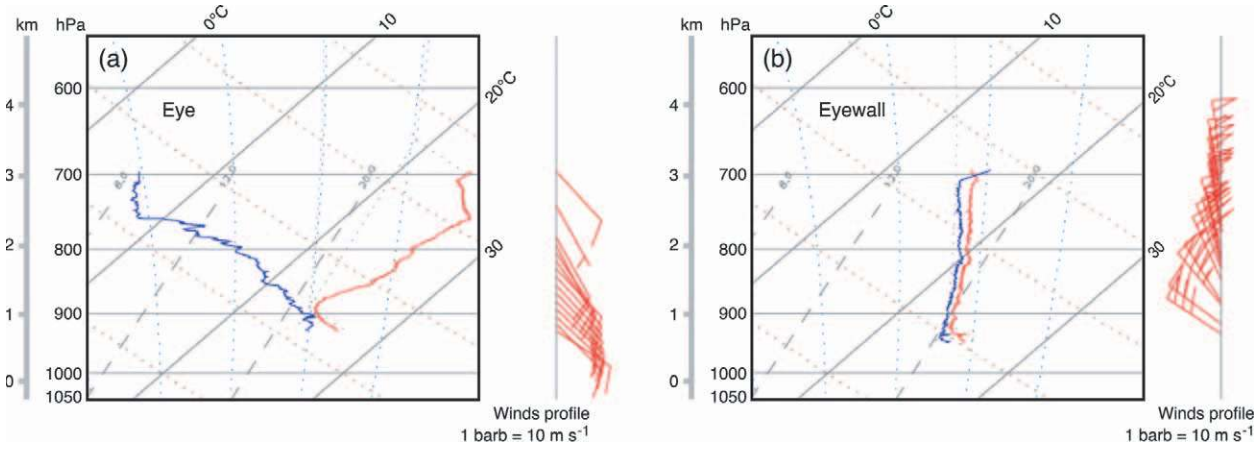

Fig. 12. Dropsonde data obtained in Hurricane Rita by the NOAA 43 aircraft (a) in the eye at 1600 UTC 21 Sep 2005 and (b) in the eyewall at 1525 UTC 21 Sep 2005. Temperature is in red; dewpoint is in blue.

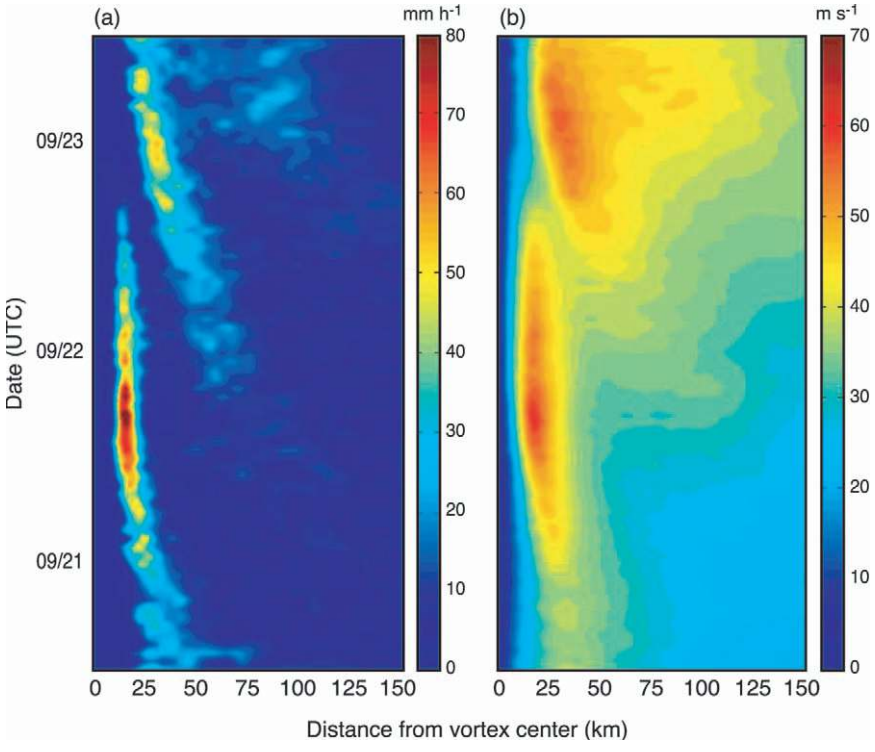

Fig. 13. Time–radius cross sections of the MM5 5-day forecast initialized at 0000 UTC 20 Sep 2005: (a) azimuthal averaged rain rate and (b) tangential wind speed at about the 3-km level.

ary eyewall on 22 September. It then contracted and eventually replaced the old inner eyewall and became the primary eyewall.

The eyewall replacement process actually occurred during the RAINEX flights on 22 September. The TRMM satellite's Precipitation Radar (PR) captured the storm in detail, at the beginning of the aircraft missions on 22 September. Figure 14 shows the horizontal and vertical structure of the reflectivity of Rita at the time that the first aircraft was entering the storm. At this time, rainbands were coalescing into an outer ring of reflectivity and beginning to form the secondary rainband (Fig. 14a), and the inner (primary) rainband was weakening in the southeast quadrant of the storm, as can be seen in the shallower echoes on the right-hand side of the eye in Fig. 14b. Flight-level wind speed measurements from the NOAA 43 aircraft flying northwest to southeast at the 3-km level indicate the two eyewalls by the presence of a double wind maximum (Fig. 15), similar to the model forecast wind field for the same time period shown in Fig. 13b. The weakening of the eyewall on the southeast side is also evident from the lower wind speeds in the southeast quadrant of the storm (right side of the figure).

Figure 16 illustrates the three-aircraft sampling accomplished during the time of the eyewall replacement in Rita on 22 September. NRL was flying a plan B circumnavigation pattern in the moat region between the primary and secondary eyewalls. A dropsonde in the moat region (Fig. 17) showed a subsid-

ence inversion, indicating that the moat was evolving into a new eye region, and evidently suppressing the inner, older primary eyewall. At this time, N42 was flying repeated eyewall penetrations and small-scale figure-four patterns, with radial legs extending ~50 km from the eye of the hurricane. The downwind legs of N42's figure-four patterns were close enough to the edge of the outer eyewall to obtain dual-Doppler radar data in the secondary eyewall. N43 obtained samples of dual-Doppler data over a broader region by flying larger figure-four patterns, with radial legs extending ~150 km from the eye. The downwind legs of these large figure-four patterns sampled rainbands in all quadrants of the storm.

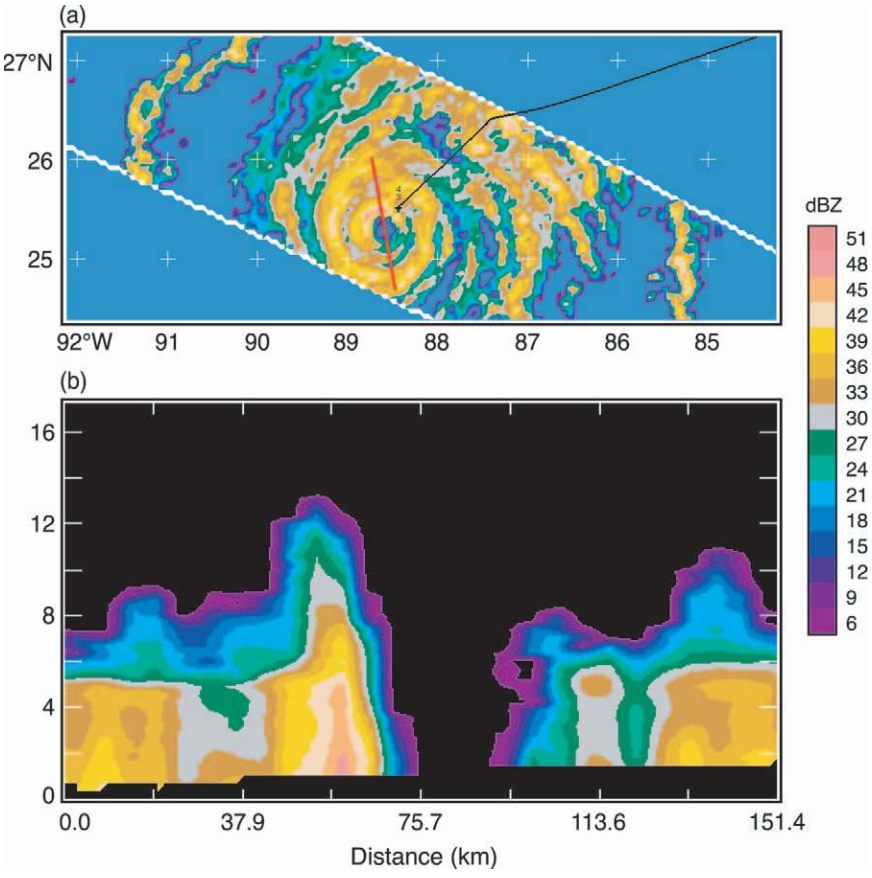

Fig. 14. Radar reflectivity data from the TRMM satellite's PR obtained in Hurricane Rita at 1445 UTC 22 Sep 2005. TRMM data are displayed by Zebra software. (a) Horizontal section at 1.75 km MSL with N43 flight track shown ending at the aircraft icon. (b) Vertical cross section left to right from north-northwest to south-southeast along the red line in (a).

A composite reflectivity image from the ELDORA radar of NRL's circumnavigation is shown in Fig. 18a. The inner eyewall (~15–20 km radius from the storm center) appeared to have been very strong on its northwest side. The complex structure within the outer eyewall (~40–50 km radius) appeared to have rainband-like qualities of relatively intense elongated echo cores embedded within the overall broad reflectivity maximum of the secondary eyewall. As in the rainband in Fig. 9, the outer eyewall had narrow, elongated echo cores oriented at a slight oblique angle to the larger, circular outer eyewall. The sizes and orientations of these narrow, oblique cores suggests a relationship to the idealized model of Kossin et al. (2000), in which barotropic instability of a circular annulus of vorticity surrounding a central core of vorticity leads to a pattern of filaments of vorticity oriented at an oblique angle to the annulus (Fig. 18b). Kossin et al. (2000) suggested that this type of vorticity structure might apply in the secondary eyewall of a tropical cyclone. Their work, however, is based on dry dynamics, and the filament-like structures seen in the real echo

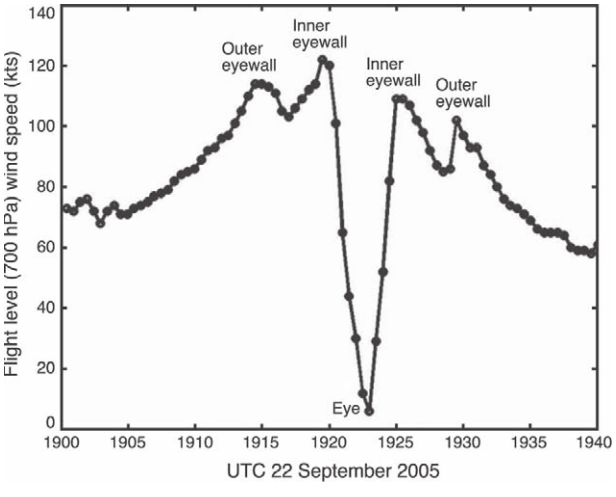

Fig. 15. Flight-level wind speed measured aboard the NOAA 43 aircraft on 22 Sep 2005 while crossing the concentric eyewalls in Hurricane Rita (as indicated by the wind maxima associated with the inner and outer eyewalls).

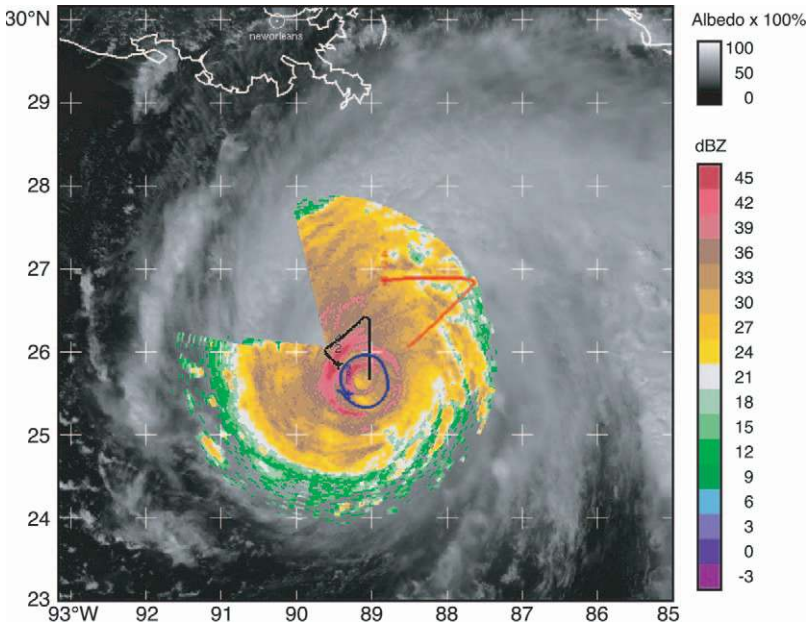

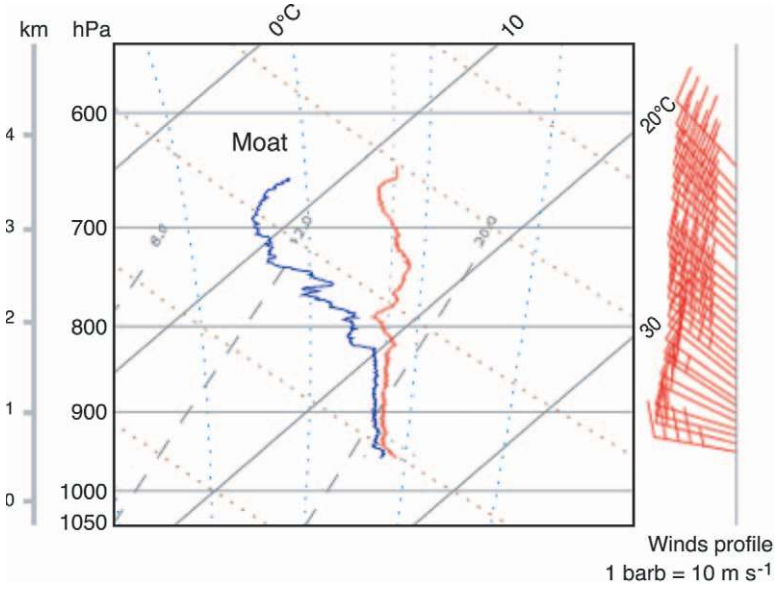

pattern in Fig. 18a may originate from another source; for example, they may be sheared moist Rossby waves or some other convectively generated cells subjected to shearing of the azimuthal wind. In any case, the finescale detail of the ELDORA radar measurements in RAINEX allows the features to be identified and compared to theoretical work.

During the day on 23 September, Rita became asymmetric as shown in both the UM high-resolution real-time model forecast (Fig. 19) and in the aircraft radar data (e.g., Fig. 20). The asymmetry was attributable to vertical wind shear over the storm. The model forecast fields showed an increase of southerly vertical wind shear over Rita from 22 to 23 September, and the rainfall asymmetry relative to the wind shear is therefore consistent with the studies of Rogers et al. (2003)

FIG. 16 (TOP). Flight tracks for NOAA 43 (red), NOAA 42 (black), and NRL (blue) ending at the aircraft icons are superimposed on lower-fuselage radar composite and visible satellite image for 1830 UTC 22 Sep 2005.

FIG. 17 (CENTER). GPS dropsonde data from the NRL P3 taken in the moat area in between the primary and secondary eyewalls in Hurricane Rita at 1800 UTC 22 Sep 2005.

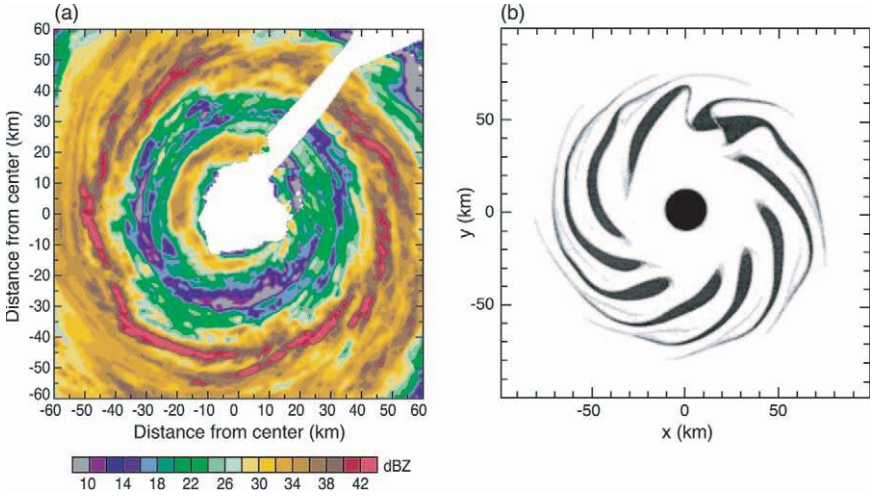

FIG. 18 (BOTTOM). (a) The 2-km ELDORA radar reflectivity composite obtained between 1712 and 1742 UTC 22 Sep 2005 for Hurricane Rita. (b) Vorticity contour plots from Kossin et al. (2000). Successively darker shading denotes successively higher vorticity. Darkest shade represents vorticity >0.003 s^{-1}. Lightest gray shade has a threshold of 0.00075 s^{-1}. High central vorticity is held constant as an initially uniform outer ring of vorticity breaks up as a result of instability. Pattern shown is 8 h after initial time.

and Chen et al. (2006a), which suggest that the maximum eyewall rainfall is to be expected in the downshear-left quadrant of the storm. The eyewall replacement on 22 September and the vertical wind shear near the landfall both probably contributed to the weakening of Rita from a category 5 to a category 3 hurricane.

CONCLUSIONS.

RAINEX observed three important 2005 hurricanes: Katrina, Ophelia, and Rita. Katrina and Rita, which were both category 5 storms over the Gulf of Mexico and reminiscent of the Great Galveston hurricane of 1900, were two of the most important storms in U.S. history. As a result of RAINEX, these storms are also among the best-documented hurricanes in history. Thirteen multi-aircraft missions were flown in these storms (Table 1), and storms were sampled in all stages ranging from tropical depression to category 5 hurricane. In Rita, an eyewall replacement was documented.

An innovative system for data transfer between a ground operations center (the ROC) and the aircraft was employed. Lower-fuselage radar data and flight-track data obtained aboard the two NOAA P3 aircraft were transmitted to the ROC and combined with satellite data to form a comprehensive real-time map at the ROC of the radar data superimposed on satellite data and flight tracks in the area of the

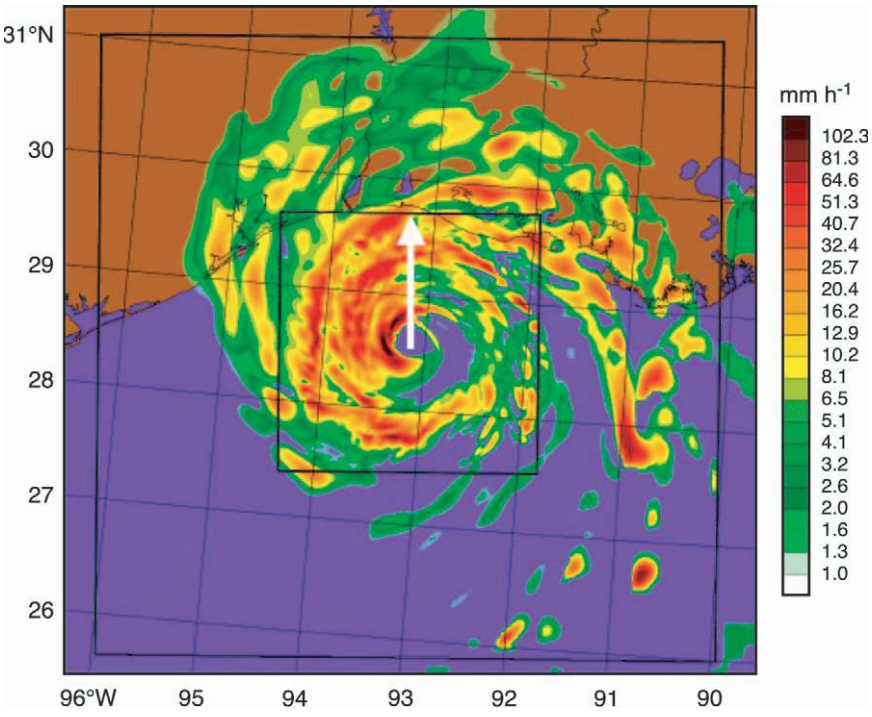

FIG. 19. MM5 forecast of rainfall rate at 0600 UTC 23 Sep 2005. The model was initialized at 0000 UTC 20 Sep. The white arrow indicates the vertical wind shear vector (200–850 hPa) from the model.

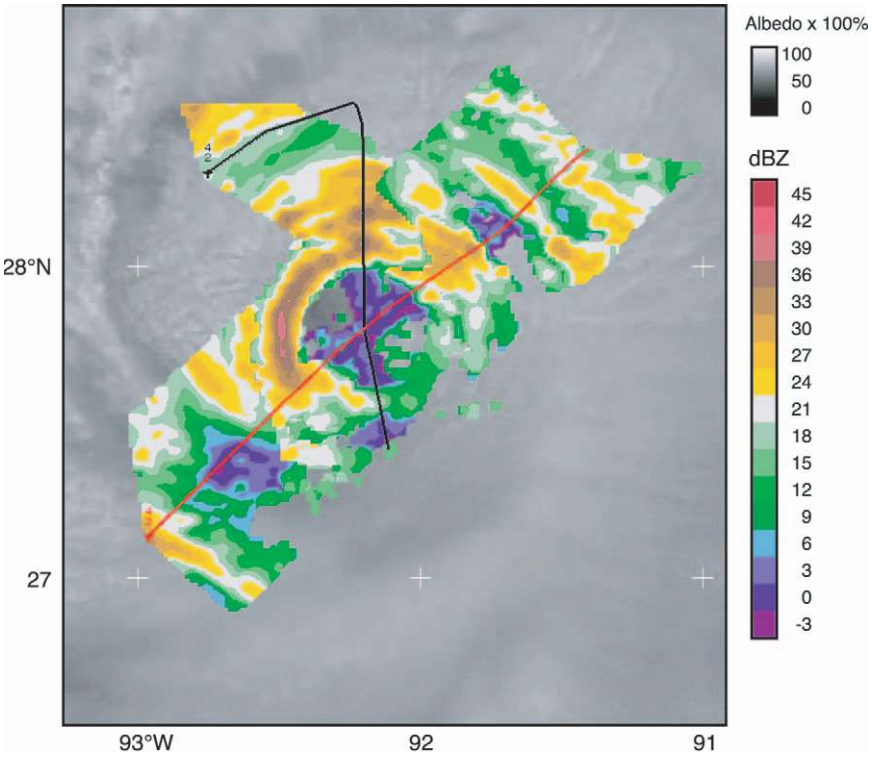

FIG. 20. N43 radar reflectivity composites obtained between 1745 and 1800 UTC 23 Sep 2005 superimposed on visible satellite data for Hurricane Rita. Flight tracks of N43 (red) and N42 (black) ending at the aircraft icons are superimposed.

storm. The ROC used these maps to position the aircraft optimally with respect to the storm, and a subset of the map was transmitted to the NRL P3 to aid in their storm navigation. Satellite-based Internet chat between the ROC and the aircraft mission scientists was particularly helpful in positioning the aircraft in relation to the map of storm structure.

RAINEX was the first experiment in which three airborne dual-Doppler radar systems were used in hurricanes. It was also the first experiment in which the higher-resolution ELDORA radar was used in a hurricane. These radar data were accompanied by upward of 1000 soundings, including 600 dropsondes targeted with the help of the ground-based operations center for optimal coordination with the airborne dual-Doppler radar observations. The comprehensive RAINEX dataset is available via the NCAR Field Catalog and RAINEX Data Archive.

A mini-ensemble forecast product set was provided in real time during RAINEX with the UM vortex-following high-resolution (~1.67 km in the inner domain) modeling system. These forecasts were remarkably accurate, reproducing both the rapid intensification of Katrina and a version of the eyewall replacement as well as the vertical wind shear in Rita. The forecasts were particularly useful in flight planning. The general accuracy of the forecasts bodes well for more detailed analysis of model simulations, taking into account the extensive sounding dataset of RAINEX. These improved simulations can then be compared with the airborne Doppler-radar data and used to analyze the mesoscale generation of PV in eyewalls and rainbands, as was the goal of RAINEX.

In this article, we have illustrated the RAINEX dataset with Hurricane Rita, in which data were obtained on five successive days, with flights documenting the tropical storm stage, the rapid intensification to category 5, an eyewall replacement, and the conversion to asymmetric storm structure when the hurricane encountered environmental wind shear. Preliminary analysis of the high-resolution ELDORA data in Rita shows convective elements oblique to rainband and eyewall structures, consistent with a secondary eyewall with small-scale internal features sheared into narrow filaments by the radially varying azimuthal wind. Preliminary analysis of the dropsonde data obtained in the eyewall replacement phase indicated that the moat between the inner and outer eyewalls was developing into a new eye region.

From the descriptions in this article, it appears that the RAINEX dataset will provide a basis for a wide range of hurricane studies over the next several years. The level of detail in the radar data, the positioning of the aircraft relative to rainbands and eyewalls, and the targeted dropsondes should provide a basis for unravelling the nature of rainbands, their interactions with eyewalls, and the relation of tropical cyclone internal structure to hurricane intensity.

ACKNOWLEDGMENTS. Carl Newman was the NRL flight program director for RAINEX and lead pilot of the NRL aircraft. His leadership was responsible for the success of the NRL P3's first hurricane flights. James MacFadden, P3 Program Manager of NOAA/AOC, tirelessly worked to make the NOAA P3 aircraft available for RAINEX flights, even after his home was without power for two weeks as a result of Katrina. Paul Chang of NOAA/NESDIS facilitated the success of RAINEX by merging the objectives of the NESDIS Ocean Winds and Rain Experiment flights of N42 with those of RAINEX. He and Dr. James Carswell of Remote Sensing Solutions, Inc., provided important engineering support for the satellite transmission of radar data from the NOAA P3 aircraft to the ROC. Chris Burghart and Janet Scannel of NCAR developed and implemented the software used in the construction of real-time mission maps at the ROC and the real-time transmission of these maps to the NRL aircraft. John Cangialosi and Derek Ortt of UM provided the daily forecasts for flight planning. Michael Anderson of UM provided crucial technical support of the ROC. Eric Loew, Michael Strong, and Hua-Qing Cai of NCAR kept ELDORA operating flawlessly and processed the ELDORA data throughout RAINEX. Errol Korn of NCAR managed the NRL P3 dropsonde program throughout RAINEX. Bradley Smull of UW, Michael Black of NOAA/HRD, and David Jorgensen of NOAA/NSSL provided crucial leadership as airborne mission scientists. José Meitín provided Web site support and coordination between the ROC and the aircraft operators. David Nolan helped with daily plannings at the ROC. Candace Gudmundson edited the manuscript and Beth Tully refined the figures. This research was supported by NSF Grants ATM-0432623 and ATM-0432717.

REFERENCES

Atlas, D., K. Hardy, R. Wexler, and R. Boucher, 1963: The origin of hurricane spiral bands. *Geofis. Int.,* **3,** 123–132.

Barnes, G. M., and G. L. Stossmeister, 1986: The structure and decay of a rainband in Hurricane Irene (1981). *Mon. Wea. Rev.,* **114,** 2590–2601.

——, E. J. Zipser, D. P. Jorgensen, and F. D. Marks Jr., 1983: Mesoscale and convective structure of a hurricane rainband. *J. Atmos. Sci,* **40,** 2125–2137.

——, J. F. Gamache, M. A. LeMone, and G. J. Stossmeister, 1991: A convective cell in a hurricane rainband. *Mon. Wea. Rev.,* **119,** 776–794.

Black, M. L., and H. E. Willoughby, 1992: A concentric eyewall cycle of Hurricane Gilbert. *Mon. Wea. Rev.,* **120,** 947–957.

——, J. F. Gamache, F. D. Marks, C. E. Samsury, and H. E. Willoughby, 2002: Eastern Pacific Hurricanes Jimena of 1991 and Olivia of 1994: The effects of vertical shear on structure and intensity. *Mon. Wea. Rev.,* **130,** 2291–2312.

Black, P. G., and F. D. Marks, 1991: The structure of an eyewall meso-vortex in Hurricane Hugo (1989). Preprints, *19th Conf. on Hurricanes and Tropical Meteorology,* Miami, FL, Amer. Meteor. Soc., 579–582.

Bosart, L. F., C. S. Velden, W. E. Bracken, J. Molinari, and P. G. Black, 2000: Environmental influences on the rapid intensification of Hurricane Opal (1995) over the Gulf of Mexico. *Mon. Wea. Rev.,* 1**28,** 322–352.

Camp, J. P., and M. T. Montgomery, 2001: Hurricane maximum intensity: Past and present. *Mon. Wea. Rev.,* **129,** 1704–1717.

Carr, L. E., and R. T. Williams, 1989: Barotropic vortex stability to perturbations from axisymmetry. *J. Atmos. Sci.,* **46,** 3177–3191.

Chen, S. S., J. A. Knaff, and F. D. Marks Jr., 2006a: Effects of vertical wind shear and storm motion on tropical cyclone rainfall asymmetries deduced from TRMM. *Mon. Wea. Rev.,* in press.

——, W. Zhao, M. A. Donelan, J. F. Price, E. J. Walsh, T. B. Sanford, and H. L. Tolman, 2006b: Fully coupled atmosphere–wave–ocean modeling for hurricane research and prediction: Results from CBLAST-Hurricane. *Bull. Amer. Meteor. Soc.,* submitted.

Chen, Y., and M. K Yau, 2001: Spiral bands in a simulated hurricane. Part I: Vortex Rossby wave verification. *J. Atmos. Sci.,* **58,** 2128–2145.

——, G. Brunet, and M. K. Yau, 2003: Spiral bands in a simulated hurricane. Part II: Wave activity diagnostics. *J. Atmos. Sci.,* **60,** 1239–1256.

Corbet, J., C. Mueller, C. Burghart, K. Gould, and G. Granger, 1994: Zeb: Software for geophysical data integration, display, and management of diverse environmental datasets. *Bull. Amer. Meteor. Soc.,* **75,** 783–792.

DeMaria, M., 1996: The effect of vertical shear on tropical cyclone intensity change. *J. Atmos. Sci.,* **53,** 2076–2087.

——, and J. Kaplan, 1994: Sea surface temperature and the maximum intensity of the Atlantic tropical cyclones. *J. Climate,* **7,** 1324–1334.

Dunion, J. P., and C. S. Velden, 2004: The impact of the Sahara air layer on Atlantic tropical cyclone activity. *Bull. Amer. Meteor. Soc.,* **85,** 353–365.

Eliassen, A., 1951: Slow thermally or frictionally controlled meridional circulation in a circular vortex. *Astrophys. Norv.,* **5,** 19–60.

Elsberry, R. L., and R. A. Jeffries, 1996: Vertical wind shear influence on tropical cyclone formation and intensification during TCM-92 and TCM-93. *Mon. Wea. Rev.,* **124,** 1374–1387.

Emanuel, K. A., 1986: An air–sea interaction theory for tropical cyclones. Part I: Steady-state maintenance. *J. Atmos. Sci.,* **43,** 585–604.

——, 1988: The maximum intensity of hurricanes. *J. Atmos. Sci.,* **45,** 1143–1155.

Evans, J. L., 1993: Sensitivity of tropical cyclone intensity to sea surface temperature. *J. Climate,* **6,** 1133–1140.

Frank, N. L., 2003: The Great Galveston Hurricane of 1900. *Hurricane! Coping With Disaster,* R. Simpson, Ed., Amer. Geophys. Union, 129–140.

Frank, W. M., and E. A. Ritchie, 1999: Effects of environmental flow upon tropical cyclone structure. *Mon. Wea. Rev.,* **127,** 2044–2061.

Frush, C. L., P. H. Hildebrand, and C. Walther, 1986: The NCAR airborne Doppler radar. Part II: System design considerations. Preprints, *23d Conf. on Radar Meteorology,* Snowmass, CO, Amer. Meteor. Soc., 151–154.

Gamache, J. F., R. A. Houze Jr., and F. D. Marks Jr., 1993: Dual-aircraft investigation of the inner core of Hurricane Norbert. Part III: Water budget. *J. Atmos. Sci.,* **50,** 3221–3243.

Guinn, T. A., and W. H. Schubert, 1993: Hurricane spiral bands. *J. Atmos. Sci.,* **50,** 3380–3403.

Hildebrand, P. H., 1989: Airborne Doppler radar accuracy. Preprints, *24th Conf. on Radar Meteorology,* Tallahassee, FL, Amer. Meteor. Soc., 585–588.

——, and Coauthors, 1996: The ELDORA/ASTRAIA Airborne Doppler Weather Radar: High-resolution observations from TOGA COARE. *Bull. Amer. Meteor. Soc.,* **77,** 213–232.

Holland, G. J., 1997: The maximum potential intensity of tropical cyclones. *J. Atmos. Sci.,* **54,** 2519-2541.

——, and G. S. Dietachmayer, 1993: On the interaction of tropical cyclone-scale vortices. III: Continuous barotropic vortices. *Quart. J. Roy. Meteor. Soc.,* **119,** 1381–1398.

Houze, R. A., Jr., 1993: *Cloud Dynamics.* Academic Press, 573 pp.

——, F. D. Marks Jr., and R. A. Black, 1992: Dual-aircraft investigation of the inner core of Hurricane Norbert. Part II: Mesoscale distribution of ice particles. *J. Atmos. Sci.,* **49,** 943–962.

Jorgensen, D. P., 1984a: Mesoscale and convective scale characteristics of mature hurricanes. Part I: General

observations by research aircraft. *J. Atmos. Sci.,* **41,** 1268–1285.

——, 1984b: Mesoscale and convective scale characteristics of mature hurricanes. Part II: Inner core structure of Hurricane Allen (1980). *J. Atmos. Sci,* **41,** 1287–1311.

——, and B. F. Smull, 1993: Mesovortex circulations seen by airborne Doppler radar within a bow-echo mesoscale convective system. *Bull. Amer. Meteor. Soc.,* **74,** 2146–2157.

——, E. J. Zipser, and M. A. LeMone, 1985: Vertical motions in intense hurricanes. *J. Atmos. Sci,* **42,** 839–856.

——, T. Matejka, and J. D. DuGranrut, 1996: Multi-beam techniques for deriving wind fields from airborne Doppler radars. *Meteor. Atmos. Phys.,* **59,** 83–104.

Kossin, J. P., and M. D. Eastin, 2001: Two distinct regimes in the kinematic and thermodynamic structure of the hurricane eye and eyewall. *J. Atmos. Sci.,* **58,** 1079–1090.

——, W. H. Schubert, and M. T. Montgomery, 2000: Unstable interactions between a hurricane's primary eyewall and a secondary ring of enhanced vorticity. *J. Atmos. Sci.,* **57,** 3890–3917.

Krishnamurti, T. N., W. N. Han, B. Jha, and H. S. Bedi, 1998: Numerical prediction of Hurricane Opal. *Mon. Wea. Rev.,* **126,** 1347–1363.

Kurihara, Y., 1976: On the development of spiral bands in a tropical cyclone. *J. Atmos. Sci.,* **33,** 940–958.

Larson, E., 1999: *Isaac's Storm.* Vintage Books, 323 pp.

Lawrence, M. B., B. M. Mayfield, L. A. Avila, R. J. Pasch, and E. N. Rappaport, 1998: Atlantic hurricane season of 1995. *Mon. Wea. Rev.,* **126,** 1124–1151.

Marks, F. D., Jr., and R. A. Houze Jr., 1984: Airborne Doppler-radar observations in Hurricane Debby. *Bull. Amer. Meteor. Soc.,* **65,** 569–582.

——, and ——, 1987: Inner core structure of Hurricane Alicia from airborne Doppler-radar observations. *J. Atmos. Sci.,* **44,** 1296–1317.

——, ——, and J. F. Gamache, 1992: Dual-aircraft investigation of the inner core of Hurricane Norbert. Part I: Kinematic structure. *J. Atmos. Sci.,* **49,** 919–942.

May, P. T., and G. J. Holland, 1999: The role of potential vorticity generation in tropical cyclone rainbands. *J. Atmos. Sci.,* **56,** 1224–1228.

Montgomery, M. T., and R. J. Kallenbach, 1997: A theory for vortex Rossby-waves and its application to spiral bands and intensity changes in hurricanes. *Quart. J. Roy. Meteor. Soc.,* **123,** 435–465.

——, and J. Enagonio, 1998: Tropical cyclogenesis via convectively forced vortex Rossby waves in a three-dimensional quasigeostrophic model. *J. Atmos. Sci.,* **55,** 3176–3207.

Muramatsu, T., 1986: Trochoidal motion of the eye of Typhoon 8019. *J. Meteor. Soc. Japan,* **64,** 259–272.

Nolan, D. S., and M. T. Montgomery, 2002: Nonhydrostatic, three-dimensional perturbations to balance, hurricane-like vortices. Part I: Linearized formulation, stability, and evolution. *J. Atmos. Sci,* **59,** 2989–3020.

——, and L. D. Grasso, 2003: Nonhydrostatic, three-dimensional perturbations to balanced, hurricane-like vortices. Part II: Symmetric response and nonlinear simulations. *J. Atmos. Sci.,* **60,** 2717–2745.

Peng, M. S., B.-F. Jeng, and R. T. Williams, 1999: A numerical study on tropical cyclone intensification. Part I: Beta effect and mean flow effect. *J. Atmos. Sci.,* **56,** 1404–1423.

Pfeffer, R. L., 1958: Concerning the mechanics of hurricanes. *J. Meteor.,* **15,** 113–120.

Powell, M. D., 1990a: Boundary-layer structure and dynamics in outer hurricane rainbands. Part I: Mesoscale rainfall and kinematic structure. *Mon. Wea. Rev.,* **118,** 891–917.

——, 1990b: Boundary-layer structure and dynamics in outer hurricane rainbands. Part II: Downdraft modification and mixed layer recovery. *Mon. Wea. Rev.,* **118,** 918–938.

Reasor, P. D., M. T. Montgomery, F. D. Marks, and J. F. Gamache, 2000: Low-wavenumber structure and evolution of the hurricane inner core observed by airborne dual-Doppler radar. *Mon. Wea. Rev.,* **128,** 1653–1680.

Rogers, R., S. S. Chen, J. E. Tenerelli, and H. E. Willoughby, 2003: A numerical study of the impact of vertical shear on the distribution of rainfall in Hurricane Bonnie (1998). *Mon. Wea. Rev.,* **131,** 1577–1599.

Samsury, C. E., and E. J. Zipser, 1995: Secondary wind maxima in hurricanes: Airflow and relationship to rainbands. *Mon. Wea. Rev.,* **123,** 3502–3517.

Schubert, W. H., M. T. Montgomery, R. K. Taft, T. A. Guinn, S. R. Fulton, J. P. Kossin, and J. P. Edwards, 1999: Polygonal eyewalls asymmetric eye contraction, and potential vorticity mixing in hurricanes. *J. Atmos. Sci.,* **56,** 1197–1223.

Shapiro, L. J., and H. E. Willoughby, 1982: The response of balanced hurricanes to local sources of heat and momentum. *J. Atmos. Sci.,* **39,** 378–394.

——, and M. T. Montgomery, 1993: A three-dimensional balance theory for rapidly rotating vortices. *J. Atmos. Sci.,* **50,** 3322–3335.

Wakimoto, R. M., W.-C. Lee, H. B. Bluestein, C.-H. Liu, and P. H. Hildebrand, 1996: ELDORA observations during VORTEX 95. *Bull. Amer. Meteor. Soc.,* **77,** 1465–1481.

Wang, Y., 2002: Vortex Rossby waves in a numerically simulated tropical cyclone. Part II: The role in tropical cyclone structure and intensity changes. *J. Atmos. Sci.,* **59,** 1239–1262.

Willoughby, H. E., 1978: A possible mechanism for the formation of hurricane rainbands. *J. Atmos. Sci.,* **35,** 838–848.

——, 1988: The dynamics of the tropical hurricane core. *Aust. Meteor. Mag.,* **36,** 183–191.

——, 1990: Temporal changes of the primary circulation in tropical cyclones. *J. Atmos. Sci.,* **47,** 242–264.

——, J. A. Clos, and M. G. Shoreibah, 1982: Concentric eyewalls, secondary wind maxima, and the evolution of the hurricane vortex. *J. Atmos. Sci.,* **39,** 395–411.

——, F. D. Marks, and R. J. Feinberg, 1984: Stationary and moving convective bands in hurricanes. *J. Atmos. Sci.,* **41,** 3189–3211.